Inorganic Chemistry

Article

pubs.acs.org/IC

Low Oxidation State Iron(0), Iron(I), and Ruthenium(0) Dinitrogen Complexes with a Very Bulky Neutral Phosphine Ligand

Ryan Gilbert-Wilson,[†] Leslie D. Field,*[,†] Stephen B. Colbran,[†] and Mohan M. Bhadbhade[‡]

[†]School of Chemistry and [‡]Mark Wainwright Analytical Center, The University of New South Wales, New South Wales 2052, Australia

Supporting Information

ABSTRACT: The synthesis of a series of iron and ruthenium complexes with the ligand $P^2P_3^{Cy}$, $P(CH_2CH_2PCy_2)_3$ is described. The iron(0) and ruthenium(0) complexes $Fe(N_2)(P^2P_3^{Cy})$ (**1**) and $Ru(N_2)(P^2P_3^{Cy})$ (**2**) were synthesized by treatment of $[FeCl(P^2P_3^{Cy})]^+$ and $[RuCl(P^2P_3^{Cy})]^+$ with an excess of potassium graphite under a nitrogen atmosphere.

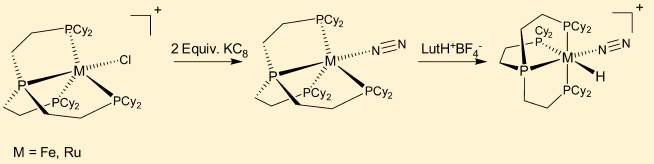

The Fe(I) and Ru(I) species $[Fe(N_2)(P^2P_3^{Cy})]^+$ (**3**) and $RuCl(P^2P_3^{Cy})$ (**4**) were synthesized by treatment of $[FeCl(P^2P_3^{Cy})]^+$ and $[RuCl(P^2P_3^{Cy})]^+$ with 1 equiv of potassium graphite under a nitrogen atmosphere. The cationic dinitrogen species $[Fe(N_2)H(P^2P_3^{Cy})]^+$ (**6**) and $[Ru(N_2)H(P^2P_3^{Cy})]^+$ (**7**) were formed by treatment of **1** and **3**, respectively, with 1 equiv of a weak organic acid. The iron(II) complex $Fe(H)_2(P^2P_3^{Cy})$ (**5**) was also synthesized and characterized. Complexes $[RuCl(P^2P_3^{Cy})][BPh_4]$, **1**, **2**, **3**[$BPh_4$], **4**, **5**, **6**[$BF_4$], and **7**[$BF_4$] were characterized by X-ray crystallography. The Fe(I) and Ru(I) complexes **3** and **4** were characterized by electron paramagnetic resonance (EPR) spectroscopy, and the Fe(I) complex has an EPR spectrum typical of a metal-centered radical.

INTRODUCTION

The first dinitrogen complexes were identified in 1965,[1] and dinitrogen complexes have since proliferated with the synthesis of a wide variety of transition metal complexes of dinitrogen.[2] Transition metal dinitrogen complexes which contain a sterically hindered ligand environment around the metal stabilize and protect the reactive metal center, producing interesting reaction chemistry.[3] In this paper, we report the use of the very hindered tripodal tetradentate phosphine ligand $P^2P_3^{Cy}$,[4] ($P(CH_2CH_2PCy_2)_3$) to produce a range of previously unknown iron and ruthenium complexes containing bound dinitrogen. The polydentate polyphosphine ligands $P(CH_2CH_2PR_2)_3$ (PP_3) are known with phenyl,[5] methyl,[6] isopropyl,[7] *tert*-butyl,[8] and cyclohexyl[9] substituents on the terminal phosphine donors. The PP_3-type ligands form strong complexes with Fe and Ru centers and are known to support dinitrogen bound at the metal center. While the low oxidation state iron and ruthenium dinitrogen complexes have been explored with the less sterically encumbered PP_3 ligands with methyl[6] and isopropyl[7] substituents, the more sterically encumbered *tert*-butyl and cyclohexyl derivatives have not yet been studied.

There are now a number of examples in the literature of iron(0) dinitrogen complexes reacting with acid to give "fixed" dinitrogen in the form of NH_3 and N_2H_4. Complexes such as $Fe(N_2)(dmpe)_2$ (dmpe = $Me_2PCH_2CH_2PMe_2$),[10] $Fe(N_2)(NP_3)$ (NP_3 = $N(CH_2CH_2PPh_2)_3$),[3b] and $Fe(DMeOPrPE)_2(N_2)$ (DMeOPrPE = 1,2-(bis-(dimethoxypropyl)phosphino)ethane)[11] have all been reported to display this reactivity. However, to date, reactivity of coordinated dinitrogen with acid has not been observed for iron(0) complexes containing podand-type ligands. When $Fe(N_2)(P^2P_3^{iPr})$ ($P^2P_3^{iPr}$ = $P(CH_2CH_2PiPr_2)_3$)[7] and $Fe(N_2)(P^2P_3^{Me})$ ($P^2P_3^{Me}$ = $P(CH_2CH_2PMe_2)_3$)[12] react with acid, the result is the protonation of the metal center to give the stable iron(II) hydrido nitrogen complexes $[Fe(N_2)(P^2P_3)H]^+$ rather than reaction at the dinitrogen ligand. Increasing the steric bulk on the PP_3-type ligand should result in greater protection of the reactive metal center with a greater potential for reaction at the coordinated dinitrogen.

As part of our ongoing work investigating the chemistry of coordinated dinitrogen, we have now studied the synthesis and reactions of dinitrogen complexes with the $P^2P_3^{Cy}$ [$P(CH_2CH_2PCy_2)_3$] ligand. We report here the synthesis and characterization of the iron(0), ruthenium(0), and iron(I) dinitrogen complexes $Fe(N_2)(P^2P_3^{Cy})$ (**1**), $Ru(N_2)(P^2P_3^{Cy})$ (**2**), and $[Fe(N_2)(P^2P_3^{Cy})]^+$(**3**), with the structural characterization of **3** being the first report of a cationic dinitrogen complex of iron(I). The isolation and structure of $RuCl(P^2P_3^{Cy})$ (**4**), the first stable ruthenium(I) monomeric complex with a neutral ligand, is also discussed, and the protonation reactions of the various dinitrogen species are investigated.

RESULTS AND DISCUSSION

Tris(2-dicyclohexylphosphinoethyl)phosphine, $P(CH_2CH_2PCy_2)_3$, ($P^2P_3^{Cy}$), and the iron and ruthenium chloride complexes $[RuCl(P^2P_3^{Cy})][BPh_4]$, $[RuCl(P^2P_3^{Cy})][Cl]$, and $[FeCl(P^2P_3^{Cy})][BPh_4]$ were synthesized by literature methods.[9] While $[RuCl(P^2P_3^{Cy})][BPh_4]$ has been previously

Received: November 15, 2012
Published: February 26, 2013

   dx.doi.org/10.1021/ic3024953 | Inorg. Chem. 2013, 52, 3043−3053

synthesized by Morris et al.,[9] characterization of the complex did not include any structural analysis. Full structural analysis of $[RuCl(P^2P_3^{Cy})][BPh_4]$ is included in the Supporting Information.

Fe(N2)($P^2P_3^{Cy}$) (1) and Ru(N2)($P^2P_3^{Cy}$) (2). The iron(0) and ruthenium(0) dinitrogen complexes $Fe(N2)(P^2P_3^{Cy})$ (**1**) and $Ru(N2)(P^2P_3^{Cy})$ (**2**) were synthesized by treatment of a THF solution of $[FeCl(P^2P_3^{Cy})][BPh_4]$ or $[RuCl(P^2P_3^{Cy})][Cl]$, with potassium graphite under an atmosphere of nitrogen (Scheme 1). After workup, $Fe(N2)(P^2P_3^{Cy})$ (**1**) was obtained

Scheme 1

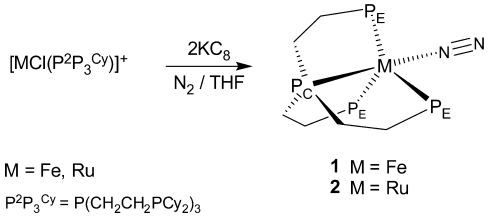

as an orange/red solid, and $Ru(N2)(P^2P_3^{Cy})$ (**2**) as a yellow solid. In the synthesis of $Fe(N2)(P^2P_3^{Cy})$ (**1**), the iron dihydride $Fe(H)_2(P^2P_3^{Cy})$ (**5**) was formed as a side product in variable amounts in addition to the desired nitrogen complex. The amount of $Fe(H)_2(P^2P_3^{Cy})$ (**5**) was decreased by shorter reaction times, but it was still necessary to use fractional crystallization to obtain $Fe(N2)(P^2P_3^{Cy})$ (**1**) of sufficient purity for characterization.

The iron(0) species $Fe(N2)(P^2P_3^{Cy})$ (**1**), unlike its iron(II) precursor $[FeCl(P^2P_3^{Cy})][BPh_4]$, is diamagnetic and has a characteristic splitting pattern in the $^{31}P\{^1H\}$ NMR spectrum for a trigonal bipyramidal complex containing a tripodal tetradentate phosphine ligand. The resonance of the central phosphine, P_C of $Fe(N_2)(P^2P_3^{Cy})$ (**1**), appears at low field at 175.3 ppm as a quartet with coupling to the three equivalent terminal phosphines P_E with a coupling constant of 36 Hz. The three equivalent terminal phosphines P_E appear as a doublet at 84.2 ppm with splitting due to P_C. In the $^{31}P\{^1H\}$ NMR spectrum of the ruthenium(0) species $Ru(N_2)(P^2P_3^{Cy})$ (**2**), the resonances of the central phosphine P_C and the three equivalent terminal phosphines P_E appear as a quartet at 160.7 ppm ($^2J_{P-P}$ = 22 Hz) and a doublet at 73.9 ppm, respectively, with the signal intensity in a ratio of 1: 3. The signals in the $^{31}P\{^1H\}$ NMR spectrum of **2** are sharp, suggestive of a trigonal bipyramidal structure in solution.

Ru($^{15}N_2$)($P^2P_3^{Cy}$) ($^{15}N_2$-2). Synthesis of $Ru(^{15}N_2)(P^2P_3^{Cy})$ (^{15}**N$_2$-2**) was performed by placing of $^{15}N_2$ gas (1.5 atm) over a degassed solution of $RuN_2(P^2P_3^{Cy})$ (**2**) in benzene-d_6.

The resolution-enhanced $^{31}P\{^1H\}$ NMR spectrum of the ^{15}N-labeled ruthenium(0) species $Ru(^{15}N_2)(P^2P_3^{Cy})$ (^{15}**N-2**) (Figure 1) clearly shows additional splitting due to the coordinated $^{15}N_2$ ligand. The resonance of the central phosphorus, P_C of ^{15}**N$_2$-2**, appears as a doublet of quartets of doublets at 160.8 ppm and that of the terminal P_E phosphines as a doublet of doublet of doublets at 74.0 ppm. The assignment of the $^{31}P-^{15}N$ coupling constants is based on the premise that the absolute value of the $^2J_{P-N}$ coupling is larger than that for the $^3J_{P-N}$ coupling.[13] The $^2J_{P-N}$ coupling constant of the P_C resonance (31 Hz) is significantly greater than the $^2J_{P-P}$ coupling constant (22 Hz) and an order of magnitude greater than the $^3J_{P-N}$ coupling constant (3 Hz). The order of magnitude difference between $^2J_{P-N}$ and $^3J_{P-N}$ *trans* coupling

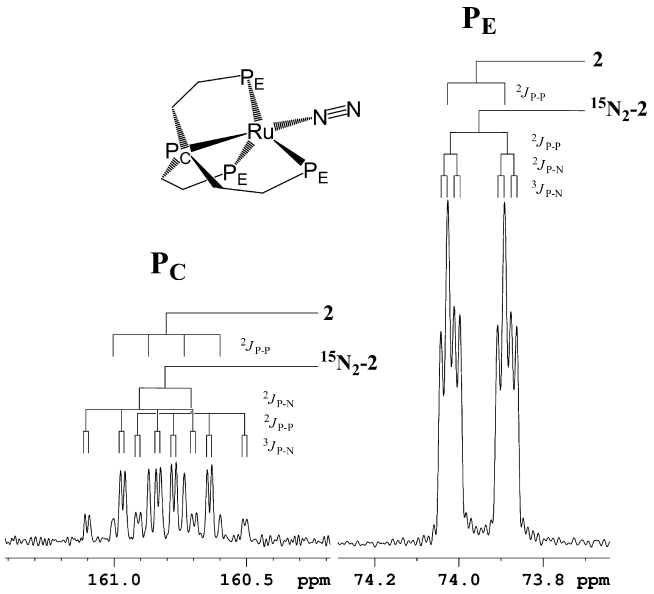

Figure 1. $^{31}P\{^1H\}$ NMR spectrum (162 MHz, C_6D_6, 298 K) of $Ru(^{15}N_2)(P^2P_3^{Cy})$ (^{15}**N$_2$-2**).

constants has been previously noted across the ruthenium center of a pyrazolyl phosphine complex, chloro(triphenylphosphine)bis[bis(1-pyrazolyl)methane]ruthenium(II) chloride.[7,14] In contrast, the $^{31}P-^{15}N$ coupling constants between P_E and the coordinated dinitrogen ($^2J_{P-N}$ and $^3J_{P-N}$) are 5 and 2 Hz, respectively.

Attempts to synthesize the analogous $Fe(^{15}N_2)(P^2P_3^{Cy})$ (^{15}**N$_2$-1**) were unsuccessful as the introduction of 1.5 atm of $^{15}N_2$ gas to a degassed solution of $FeN_2(P^2P_3^{Cy})$ (**1**) gave only $FeN_2(P^2P_3^{Cy})$ (**1**) and failed to displace ^{14}N dinitrogen from the complex.

Orange crystals of $Fe(N2)(P^2P_3^{Cy})$ (**1**) suitable for analysis by X-ray diffraction were grown by slow evaporation of a benzene solution of **1** (Figure 2). Selected bond lengths and bond angles are listed in Table 1.

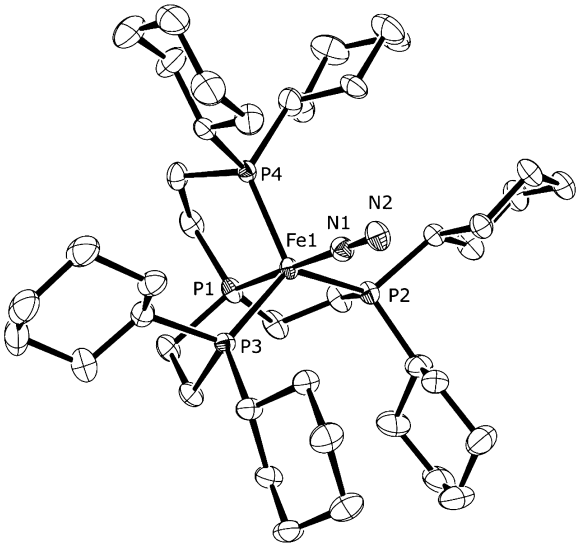

Figure 2. ORTEP diagram (50% thermal ellipsoids, non-hydrogen atoms) of $Fe(N_2)(P^2P_3^{Cy})$ (**1**) excluding benzene solvate.

dx.doi.org/10.1021/ic3024953 | Inorg. Chem. 2013, 52, 3043−3053

Table 1. Selected Bond Lengths (Å) and Angles (°) for $Fe(N_2)(P^2P_3^{Cy})$ (1)

N1−N2	1.134(3)	Fe1−N1	1.812(2)
Fe1−P1	2.1430(9)	Fe1−P2	2.2105(9)
Fe1−P3	2.2301(12)	Fe1−P4	2.1991(8)
N1−Fe1−P1	178.90(7)	N1−Fe1−P2	93.84(8)
N1−Fe1−P3	97.18(9)	N1−Fe1−P4	95.06(8)
P1−Fe1−P2	85.06(4)	P1−Fe1−P3	83.42(5)
P1−Fe1−P4	85.51(4)	P2−Fe1−P3	124.14(3)
P2−Fe1−P4	118.72(4)	P3−Fe1−P4	114.55(4)
Fe1−N1−N2	178.9(2)		

The geometry around the metal center of $Fe(N_2)(P^2P_3^{Cy})$ (**1**) approximates well to trigonal bipyramidal as demonstrated by a τ value of $\tau = 0.91$, where τ is a geometric parameter indicative of 5-coordinate complex geometry ($\tau = 0$ is perfect square pyramidal geometry and $\tau = 1$ is perfect trigonal-bipyramidal geometry).[15] The N−N triple bond length of 1.134(3) Å indicates modest activation compared to the N−N triple bond length for free dinitrogen (1.10 Å).[16] Two iron(0) dinitrogen complexes with four phosphorus donors have previously been structurally characterized, the analogous $Fe(N_2)(P^2P_3^{iPr})$ ($P^2P_3^{iPr}$ = $P(CH_2CH_2PiPr_2)_3$,[7] and $Fe(N_2)(depe)_2$ (depe = $Et_2PCH_2CH_2PEt_2$).[17] All three structures are comparable, with $Fe(N_2)(P^2P_3^{iPr})$ and $Fe(N_2)(depe)_2$ having N−N bond distances of 1.1279(16) and 1.14(1) Å respectively, compared with a N−N distance of 1.134(3) Å for **1**. All three complexes also have similar trigonal bipyramidal geometry, the only difference being that $Fe(N_2)(depe)_2$ has the dinitrogen ligand located in an equatorial position rather than the axial position of dinitrogen found in both $Fe(N_2)(P^2P_3^{Cy})$ (**1**) and $Fe(N_2)(P^2P_3^{iPr})$.

Crystals of $Ru(N_2)(P^2P_3^{Cy})$ (**2**) suitable for structural analysis were grown by cooling a saturated pentane solution at −20 °C (Figure 3). Selected bond lengths and bond angles are listed in Table 2.

The geometry about the metal center of $RuN_2(P^2P_3^{Cy})$ (**2**) is perfectly trigonal bipyramidal ($\tau = 1.0$) with the three arms of the $P^2P_3^{Cy}$ ligand being equivalent by symmetry. This is the

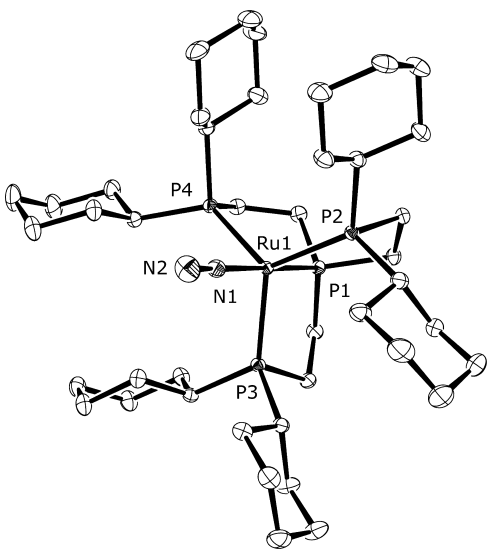

Figure 3. ORTEP plot (50% thermal ellipsoids, non-hydrogen atoms) of $RuN_2(P^2P_3^{Cy})$ (**2**) within each asymmetric unit. Pentane solvate has been omitted for clarity.

Table 2. Selected Bond Lengths (Å) and Angles (°) for $RuN_2(P^2P_3^{Cy})$ (2)

N1−N2	1.097(2)	Ru1−N1	2.0033(17)
Ru1−P1	2.2172(5)	Ru1−P2	2.3299(5)
Ru1−P3	2.3302(5)	Ru1−P4	2.3227(5)
Ru1−N1−N2	179.8(2)	P1−Ru1−N1	179.92(5)
P2−Ru1−N1	96.28(5)	P3−Ru1−N1	96.84(4)
P4−Ru1−N1	96.03(4)	P1−Ru1−P2	83.720(17)
P1−Ru1−P3	83.227(17)	P1−Ru1−P4	83.905(17)
P2−Ru1−P3	118.866(17)	P2−Ru1−P4	118.374(17)
P3−Ru1−P4	119.102(17)		

second structurally characterized ruthenium(0) dinitrogen complex with the first being the analogous $Ru(N_2)(P^2P_3^{iPr})$ ($P^2P_3^{iPr}$ = $P(CH_2CH_2P^iPr_2)_3$).[7] Both have similar ruthenium phosphine bond distances and similar levels of dinitrogen ligand activation, as evidenced by the N−N bond lengths of 1.097(2) Å for **2**, versus 1.109(4) Å for $Ru(N_2)(P^2P_3^{iPr})$. The N−N distances are similar to the bond length for free dinitrogen (1.10 Å)[16] demonstrating minimal overall N_2 activation. The lack of activation of the dinitrogen ligand suggests weak coordination, which is also consistent with the observed facile exchange of this ligand with $^{15}N_2$.

The infrared spectrum of $Fe(N_2)(P^2P_3^{Cy})$ (**1**) displays a sharp absorbance at 1996 cm^{-1} which is assigned to the nitrogen−nitrogen triple bond stretch $\nu(N{\equiv}N)$. The $\nu(N{\equiv}N)$ stretch is also a measure of the degree of activation of the N−N triple bond when bound to a metal center, with frequencies usually found between the frequency for free dinitrogen at 2331 cm^{-1} and that for a diazene derivative PhN=NPh at 1442 cm^{-1}.[2a] Monomeric iron(0) dinitrogen complexes have been identified with $\nu(N{\equiv}N)$ absorbances in the range 1830−2141 cm^{-1}.[18] In comparison to other iron(0) dinitrogen complexes, **1** has an average level of nitrogen activation, sitting slightly below the level of nitrogen activation observed for $Fe(dmpe)_2(N_2)$[19] (1975 cm^{-1}) and $Fe(DMeOPrPE)_2(N_2)$[11] (1966 cm^{-1}). It should be noted that several controlled studies have demonstrated that there is not always a correlation between the level of dinitrogen activation and the extent of nitrogen reactivity,[20] but in the case of iron complexes dinitrogen reactivity correlates reasonably well with dinitrogen activation.[18]

The infrared spectrum of $Ru(N_2)(P^2P_3^{Cy})$ (**2**) displays a sharp absorbance at 2083 cm^{-1} assigned to the nitrogen−nitrogen triple bond stretch $\nu(N{\equiv}N)$. The higher value when compared to that of $Fe(N_2)(P^2P_3^{Cy})$ (**1**) highlights the lower level of dinitrogen activation in ruthenium complexes when compared to those of analogous iron complexes. The value is comparable to that observed for other ruthenium(0) dinitrogen complexes such as $Ru(N_2)(P(CH_2CH_2P^iPr_2)_3)$ (2083 cm^{-1}).[7]

Iron(I) and Ruthenium(I) Complexes. The iron(I) dinitrogen complex $[Fe(N2)(P^2P_3^{Cy})][BPh_4]$ (**3**$[BPh_4]$) was synthesized by treatment of a THF solution of $[FeCl(P^2P_3^{Cy})][BPh_4]$ with 1 equiv of potassium graphite under an atmosphere of nitrogen (Scheme 2). After workup, **3**$[BPh_4]$ was obtained as a deep red solid.

Attempting a similar reaction to produce the ruthenium(I) dinitrogen complex was unsuccessful. Reacting 1 equiv of potassium graphite with $[RuCl(P^2P_3^{Cy})][BPh_4]$ in THF resulted in a mixture of the starting material and $Ru(N_2)(P^2P_3^{Cy})$ (**2**). Using the chloride salt $[RuCl(P^2P_3^{Cy})][Cl]$ in the place of $[RuCl(P^2P_3^{Cy})][BPh_4]$ under the same reaction

dx.doi.org/10.1021/ic3024953 | Inorg. Chem. 2013, 52, 3043−3053

Scheme 2

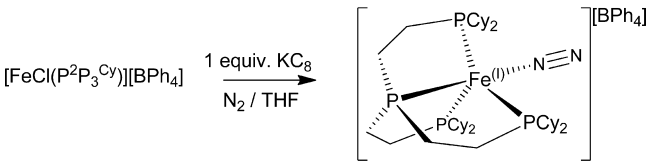

3

conditions resulted in the synthesis of the ruthenium(I) chloro complex $RuCl(P^2P_3^{Cy})$ (**4**) as a blue solid after workup (Scheme 3).

Scheme 3

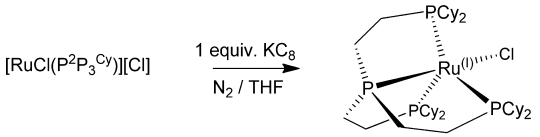

4

Until recently, there were no stable ruthenium(I) complexes known. The few Ru(I) species that had been identified were unstable species, often produced by electrochemical methods where the products were not able to be isolated. $Ru(dppp)_2Cl$ (dppp = 1,3-bisdiphenylphosphinopropane) was the first Ru(I) complex to be produced, and its instability was attributed to the presumed lability of the chloro ligand which opened facile decomposition pathways through disproportionation.[21] A longer lived complex $Ru(PP_3)Cl$ (PP_3 = $P(CH_2CH_2PPh_2)_3$) was later identified but could not be successfully isolated.[5a] The first stable ruthenium(I) compounds were isolated when anionic ligands of the type $(SiP^{iPr}_3)^-$ ($(SiP^{iPr}_3)^-$ = (2-$iPr_2PC_6H_4)_3Si^-$) imparted extra stability by having a nonlabile, charge stabilizing anionic ligand. Both $[(SiP^{iPr}_3)Ru(N_2)]$ and $[(SiP^{iPr}_3)Ru(PMe_3)]$[22] were isolated and characterized using the Si-centered anionic polydentate ligands. Our synthesis of $RuCl(P^2P_3^{Cy})$ (**4**) demonstrates that it is indeed possible to generate stable ruthenium(I) complexes even with labile chloro ligands. The increased stability in our system probably stems from the increased steric bulk of the neutral phosphine ligand, which may inhibit the interaction between ruthenium(I) centers necessary for a disproportionation reaction.

Crystals of $[Fe(N2)(P^2P_3^{Cy})][BPh_4]$ (**3**[**BPh$_4$**]) suitable for structural analysis were grown by vapor diffusion of pentane into a THF solution of **3**[**BPh$_4$**] (Figure 4). Selected bond angles and lengths are listed in Table 3.

The geometry of $[Fe(N_2)(P^2P_3^{Cy})]^+$ (**3**) is that of a distorted trigonal bipyramid with atoms P2, P3, and P4 making up the equatorial plane and P1, and N1 at the two apexes (τ = 0.91).[15] This is the first structurally characterized iron(I) dinitrogen cation, with the previous three structurally characterized iron(I) dinitrogen complexes $[Fe(SiP^{iPr}_3)(N_2)]$, $[Fe(SiP^{Ph}_3)(N_2)]$ (SiP^R_3 = $[(R_2PC_6H_4)_3Si]^-$)[23] and [2-[2,6-(^{i}Pr)$_2$PhN=C-(CH_3)]-6-[2,6-(iPr)$_2$PhN−CH=CH_2](C_5H_3N)]Fe−N_2[24] having had anionic ligands resulting in neutral complexes. $[Fe(SiP^{iPr}_3)(N_2)]$ has a similar level of distortion from trigonal bipyramidal (τ = 0.88), whereas $[Fe(SiP^{Ph}_3)(N_2)]$ is rigorously trigonal bipyramidal (τ = 1.00). The distortion away from trigonal bipyramidal is probably due to the steric influence of the bulkier isopropyl and cyclohexyl groups and the way they pack against each other, rather than the innate geometrical preferences of an iron(I) center.

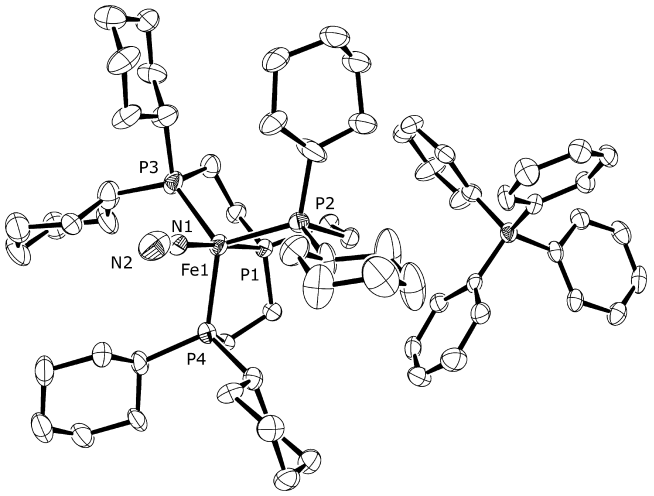

Figure 4. ORTEP diagram (50% thermal ellipsoids, non-hydrogen atoms) of $[Fe(N_2)(P^2P_3^{Cy})][BPh_4]$ (**3**[**BPh$_4$**]).

Table 3. Selected Bond Lengths (Å) and Angles (°) for $[Fe(N_2)(P^2P_3^{Cy})][BPh_4]$ (3[BPh$_4$])

N1−N2	0.987(6)	Fe1−N1	1.878(6)
Fe1−P1	2.1870(16)	Fe1−P2	2.3010(16)
Fe1−P3	2.2760(17)	Fe1−P4	2.2981(16)
N1−Fe1−P1	177.80(16)	N1−Fe1−P2	95.88(16)
N1−Fe1−P3	97.29(16)	N1−Fe1−P4	94.16(16)
P1−Fe1−P2	83.90(6)	P1−Fe1−P3	84.72(6)
P1−Fe1−P4	83.97(6)	P2−Fe1−P3	118.56(6)
P2−Fe1−P4	114.93(6)	P3−Fe1−P4	123.48(6)
Fe1−N1−N2	178.2(7)		

The infrared spectrum of $[Fe(N_2)(P^2P_3^{Cy})]^+$ (**3**) shows a sharp absorbance at 2059 cm^{-1} assigned to the nitrogen−nitrogen triple bond stretch ν(N≡N). This is less activated than the previously identified iron(I) dinitrogen complexes for which IR data are available $[Fe(N_2)(SiP^{iPr}_3)]$ (2003 cm^{-1}) and $[Fe(N_2)(SiP^{Ph}_3)]$ (2041 cm^{-1}).[23] The ν(N≡N) for **3** does however lie to the lower end of the range of ν(N≡N) values for iron(II) complexes which have been measured between 2040 and 2145 cm^{-1}.[18]

Crystals of $RuCl(P^2P_3^{Cy})$ (**4**) suitable for structural analysis were grown by slow evaporation of a concentrated pentane solution of **4** (Figure 5). Selected bond angles and lengths are listed in Table 4.

The geometry of $RuCl(P^2P_3^{Cy})$ (**4**) lies about halfway between trigonal bipyramidal and square-based pyramidal, and this is consistent with the value of τ for the structure being close to 0.5 (τ = 0.56).[15] The distorted geometry is due to the P1−Ru1−P3 angle (142.53(9)°) being much larger than the angles between the other equatorial phosphine donors P1−Ru1−P2 and P2−Ru1−P3 (108.14(9)° and 104.95(9)°), respectively, however not close enough to 180° for square-based pyramid geometry. The Ru1−Cl1 bond length in $RuCl(P^2P_3^{Cy})$ (**4**) (2.486(2) Å) is longer than that of the Ru−Cl bond in the ruthenium(II) precursor $[RuCl(P^2P_3^{Cy})][BPh_4]$ (2.4235(12) Å) as identified crystallographically (see Supporting Information). The increased Ru−Cl bond length is probably due to the decreased charge on the ruthenium atom and indicates that the chloro ligand in $RuCl(P^2P_3^{Cy})$ (**4**) is

dx.doi.org/10.1021/ic3024953 | Inorg. Chem. 2013, 52, 3043−3053

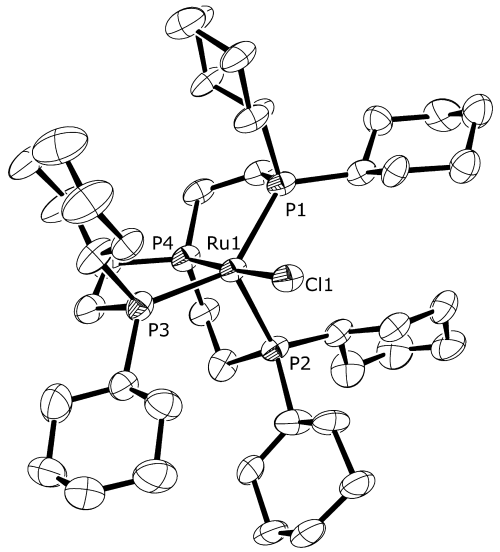

Figure 5. ORTEP diagram (50% thermal ellipsoids, non-hydrogen atoms) of RuCl($P^2P_3^{Cy}$) (**4**); pentane solvate omitted for clarity.

Table 4. Selected Bond Lengths (Å) and Angles (°) for RuCl($P^2P_3^{Cy}$) (4)

Ru1−Cl1	2.486(2)	Ru1−P1	2.356(2)
Ru1−P2	2.332(2)	Ru1−P3	2.345(3)
Ru1−P4	2.196(2)		
Cl1−Ru1−P1	95.44(8)	Cl1−Ru1−P2	99.61(8)
Cl1−Ru1−P3	95.90(8)	Cl1−Ru1−P4	176.34(9)
P1−Ru1−P2	108.14(9)	P1−Ru1−P3	142.53(9)
P1−Ru1−P4	83.28(9)	P2−Ru1−P3	104.95(9)
P2−Ru1−P4	84.05(9)	P3−Ru1−P4	83.15(9)

likely to be more labile that the chloro ligand in [RuCl($P^2P_3^{Cy}$)][BPh_4]. The increased stability of RuCl($P^2P_3^{Cy}$) (**4**) over previously identified ruthenium(I) chloro complexes is therefore not likely to be due to a decrease in chloro ligand lability and can probably best be attributed to the increased steric bulk preventing interaction between ruthenium(I) centers which could ultimately lead to decomposition through disproportionation.

There are only two other structurally characterized monomeric Ru(I) complexes [(SiP^{iPr}_3)Ru(N_2)] and [(SiP^{iPr}_3)Ru(PMe_3)],[22] both of which utilize the silicon centered ligand $(SiP^{iPr}_3)^-$ ($(SiP^{iPr}_3)^-$ = $((2\text{-}iPr_2PC_6H_4)_3Si)^-$). Both of these structures are closer to having trigonal bipyramidal geometry (τ values of 0.76 and 0.86 respectively) than RuCl($P^2P_3^{Cy}$) (**4**), but both of these structures are still significantly distorted from a pure trigonal bipyramidal geometry. The indications are that 5-coordinate ruthenium(I) complexes prefer a geometry which is neither a square pyramidal geometry like ruthenium(II) nor a trigonal bipyramidal geometry like ruthenium(0) but something midway between the two.

Although complexes [Fe(N2)($P^2P_3^{Cy}$)][BPh_4] (**3**[**BPh$_4$**]) and RuCl($P^2P_3^{Cy}$) (**4**) are formally Fe(I) and Ru(I) complexes, the possibility of a ligand-centered radical cannot be excluded based on structural studies alone, especially in light of the growing recognition of redox non-innocence of many auxiliary ligands.[25] To investigate the distribution of spin density in **3** and **4**, electron paramagnetic resonance (EPR) spectra were obtained at 77 K in THF glass (Figure 6 and the Supporting Information). Each spectrum exhibits rhombic features with hyperfine coupling to the phosphorus atoms of the ligand.

In assessing metal radical character, the anisotropy of the g values (g being a constant of proportionality, whose value is the property of the electron in a certain environment) ($\Delta g = g_{max} - g_{min}$) is particularly noteworthy, since a large Δg value has been noted as a crude indication of metalloradical character for S = 1/2 systems,[26] though there are some examples of ligand centered radicals with large Δg.[27] Proven ligand centered radicals have lower Δg in the range of 0.0575−0.0779,[28,29] with proven metal centered radicals having larger Δg in the realm of 0.197−0.252.[30]

The relatively large Δg value for[Fe(N2)($P^2P_3^{Cy}$)]$^+$ **3** of 0.226 clearly indicates a metal-centered radical, while RuCl($P^2P_3^{Cy}$) **4**, with a Δg value of 0.103 is less diagnostic. Although g values alone cannot be used as a quantitative measure of spin density, the simulated EPR parameters also support **3** and **4** being metalloradicals.

Fe(H)$_2$($P^2P_3^{Cy}$) (5). Fe(H)$_2$($P^2P_3^{Cy}$) (**5**) was first observed as a side product in the synthesis of Fe(N_2)($P^2P_3^{Cy}$) (**1**). Because Fe(H)$_2$($P^2P_3^{Cy}$) **5** was formed alongside FeN_2($P^2P_3^{Cy}$) **1** and was difficult to separate and purify, an authentic sample was synthesized by reduction of FeCl($P^2P_3^{Cy}$)][BPh_4]. FeCl($P^2P_3^{Cy}$)][BPh_4] was reacted with potassium triethylborohydride ($KBEt_3H$) in toluene (Scheme 4). Crystals suitable for structural analysis were grown by slow evaporation of a toluene solution of complex **5** (Figure 7). Selected bond angles and lengths are listed in Table 5.

The geometry of Fe(H)$_2$($P^2P_3^{Cy}$) (**5**) is distorted octahedral, with the two hydrides in a mutually *cis* arrangement. The distortion away from octahedral is due to expanded P−Fe−P bond angles between the terminal phosphines P2−Fe1−P3 and

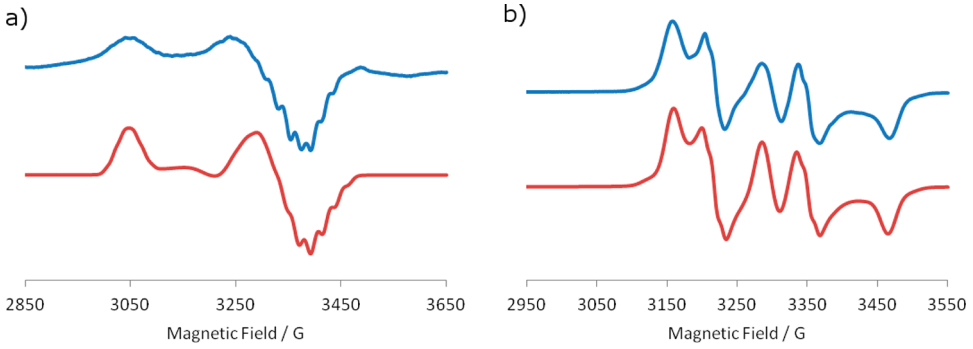

Figure 6. Experimental (upper) and simulated (lower) EPR spectra of (a) of [Fe(N2)($P^2P_3^{Cy}$)]$^+$ **3** (77 K); (g_x, g_y, g_z) = (2.225, 2.040,1.999); and (b) EPR spectrum of RuCl($P^2P_3^{Cy}$) **4** (77 K); (g_x, g_y, g_z) = (2.104, 2.064, 2.0005). See Supporting Information for other parameters.

dx.doi.org/10.1021/ic3024953 | *Inorg. Chem.* 2013, 52, 3043−3053

Scheme 4

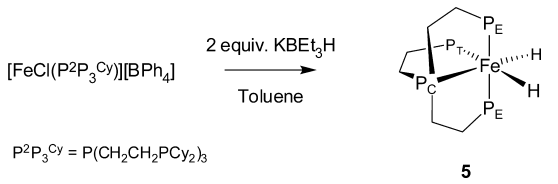

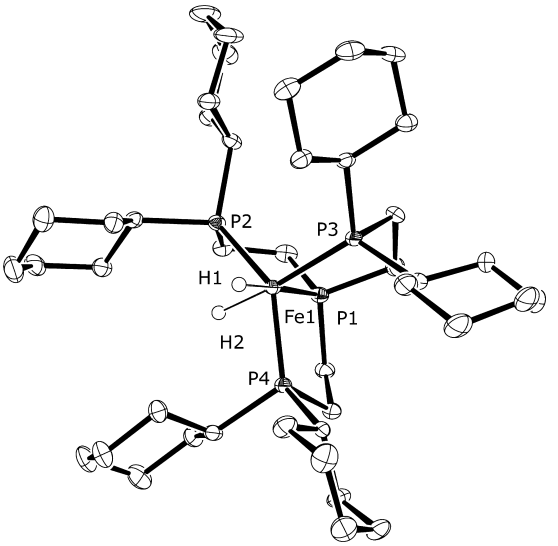

Figure 7. ORTEP plot (50% thermal ellipsoids) of $Fe(H)_2(P^2P_3^{Cy})$ (**5**) within each asymmetric unit. Selected hydrogen atoms and second complex in the asymmetric unit have been omitted for clarity.

Table 5. Selected Bond Lengths (Å) and Angles (°) for $[Fe(H)_2(P^2P_3^{Cy})]$ (5)

Fe1−H1	1.44(3)	Fe1−H2	1.47(3)
Fe1−P1	2.1108(8)	Fe1−P2	2.1776(8)
Fe1−P4	2.1766(8)	Fe1−P3	2.2036(8)
H1−Fe1−P2	94.9(12)	H1−Fe1−P1	177.6(12)
H1−Fe1−P3	94.5(11)	H1−Fe1−P4	89.9(12)
H2−Fe1−P2	65.6(11)	H2−Fe1−P1	91.2(11)
H2−Fe1−P3	173.1(11)	H2−Fe1−P4	75.7(11)
P1−Fe1−P2	86.85(3)	P2−Fe1−P3	107.76(3)
P2−Fe1−P4	140.77(3)	P1−Fe1−P3	86.35(3)
P1−Fe1−P4	87.75(3)	P3−Fe1−P4	110.61(3)
H1−Fe1−H2	88.1(15)		

P3−Fe1−P4 (>105°), resulting in compressed H2−Fe1−P2 and H2−Fe1−P4 bond angles. Three other iron dihydride complexes with phosphine ligands have been previously characterized crystallographically[31] with $Fe(H)_2(Ph_2PCH_2CH_2PPh_2)_2$[31a] and $Fe(H)_2[(PhP(OC_2H_5)_2]_4$[31b] both also being complexes having mutually *cis* hydrido ligands. $Fe(H)_2(Ph_2PCH_2CH_2PPh_2)_2$, $Fe(H)_2[(PhP(OC_2H_5)_2]_4$, and $Fe(H)_2(P^2P_3^{Cy})$ (**5**) all share similar distorted octahedral geometry with much smaller P−Fe−H bond angles than P−Fe−P bond angles. These compressed P−Fe−H bond angles can be attributed to the small size of the hydride ligands, which allows the bulkier phosphines to relieve steric strain by moving toward the hydrides. The small differences observed in bond lengths and angles can be attributed to the different denticity of the ligands in all three complexes resulting indifferent steric constraints on the final structure.

The $^{31}P\{^1H\}$ NMR spectrum of $Fe(H)_2(P^2P_3^{Cy})$ (**5**) contains only two sharp resonances at 315 K, a quartet at 174.4 ppm assigned to the central phosphine P_C and a doublet at 102.3 ppm assigned to the terminal phosphines $P_{E/T}$ in a 1:3 ratio, with a $^{31}P-^{31}P$ coupling constant of 18 Hz (Figure 8).

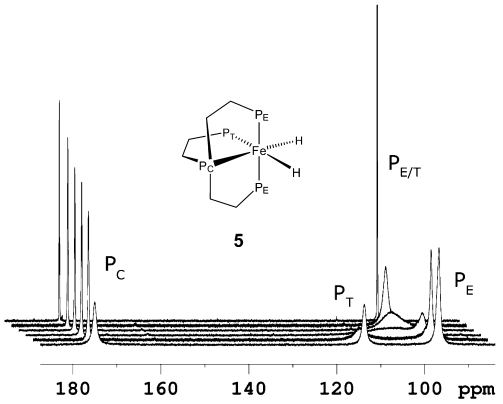

Figure 8. Variable temperature $^{31}P\{^1H\}$ NMR spectra (600 MHz, toluene-d_8) of $Fe(H)_2(P^2P_3^{Cy})$ (**5**) with spectra at (from front) at 190, 210, 225, 240, 254, and 315 K.

This spectrum is consistent with fast exchange occurring between the terminal phosphorus environments, P_E and P_T. At 240 K, the exchange is slowed causing significant broadening of the $P_{E/T}$ resonance. As the temperature is lowered further to 190 K, two distinct broad resonances emerge at δ 96.8 and δ 113.7 for the two P_E and one P_T phosphine atoms respectively (Figure 8).

The ^1H NMR spectrum of $Fe(H)_2(P^2P_3^{Cy})$ (**5**) shows a corresponding exchange with the two hydride signals in fast exchange at 285 K (Figure 9) giving rise to a single sharp

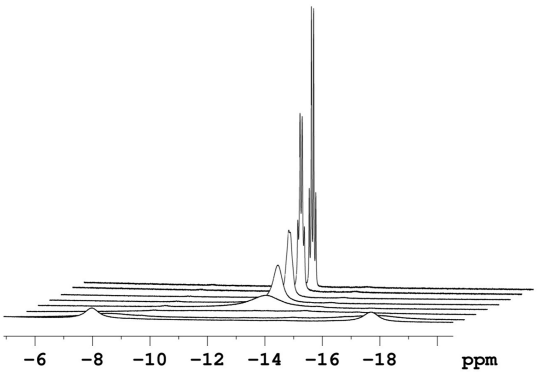

Figure 9. Variable temperature ^1H NMR spectra (600 MHz, toluene-d_8) of the high field region of $Fe(H)_2(P^2P_3^{Cy})$ (**5**) with spectra at (from front) 190, 200, 210, 225, 240, 254, 271, and 285 K.

resonance at −12.84 ppm. At 240 K, the hydride resonance was broadened to the point where $^2J_{H-P}$ coupling could no longer be observed. At 210 K two broad resonances appeared at −7.95 and −17.71 ppm, with these resonances becoming significantly sharper at 190 K (Figure 9).

The iron dihydride $Fe(H)_2(P^2P_3^{Cy})$ (**5**) has a faster rate of exchange than that observed for the analogous dihydride $Fe(H)_2(P^2P_3^{Me})$ ($P^2P_3^{Me}$ = $P(CH_2CH_2PMe_2)_3$).[6b] This supports previous discussion that the mechanism of exchange for iron dihydrides with tetradentate phosphine ligands was most

dx.doi.org/10.1021/ic3024953 | Inorg. Chem. 2013, 52, 3043−3053

likely a process of temporary detachment of one of the bound phosphines to give a five coordinate complex which could undergo facile pseudorotation before recoordination of the fourth phosphine. This process would be accelerated by increased steric bulk on the terminal phosphines as the steric repulsion between the terminal phosphines would increase, lowering the barrier for detachment.

Reactivity of Dinitrogen Complexes. Treatment of the iron(0) and ruthenium(0) dinitrogen species $Fe(N2)(P^2P_3{}^{Cy})$ (**1**) and $Ru(N_2)(P^2P_3{}^{Cy})$ (**2**) with 1 equiv of the weak organic acid 2,6-lutidinium tetrafluoroborate results in protonation of the metal centers to give the iron(II) and ruthenium(II) dinitrogen hydride complexes $[FeH(N_2)(P^2P_3{}^{Cy})]^+$ (**6**) and $[RuH(N_2)(P^2P_3{}^{Cy})]^+$ (**7**), respectively (Scheme 5). $[FeH(N_2)(P^2P_3{}^{Cy})]^+$ (**6**) could also be generated by the treatment of $Fe(H)_2(P^2P_3{}^{Cy})$ (**5**) with 1 equiv of 2,6-lutidinium tetrafluoroborate under a nitrogen atmosphere, and it was this synthetic method which was used to synthesize samples for characterization purposes. $[FeH(N_2)(P^2P_3{}^{Cy})]^+$ (**6**) and $[RuH(N_2)(P^2P_3{}^{Cy})]^+$ (**7**) are both stable with respect to further protonation with 2,6-lutidinium tetrafluoroborate. Reaction of $Fe(N2)(P^2P_3{}^{Cy})$ (**1**) and $Ru(N2)(P^2P_3{}^{Cy})$ (**2**) with an excess of stronger acids such as hydrochloric acid and triflic acid leads to protonation of the phosphine ligand and no identifiable products of reaction at the coordinated nitrogen. Treatment of $[Fe(N2)(P^2P_3{}^{Cy})][BPh_4]$ (**3**[**BPh**$_4$]) with 1 equiv of acid, either 2,6-lutidinium tetrafluoroborate or fluoroboric acid, resulted in the very slow synthesis of $[FeH(N_2)(P^2P_3{}^{Cy})]^+$ (**6**) most likely through acid assisted disproportionation.

Scheme 5

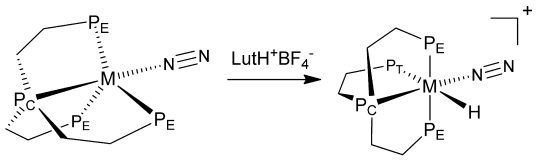

1 M = Fe
2 M = Ru

6 M = Fe
7 M = Ru

M = Fe, Ru

$P^2P_3{}^{Cy} = P(CH_2CH_2PCy_2)_3$

$[FeH(N_2)(P^2P_3{}^{Cy})]^+$ (**6**) is analogous to the known iron(II) dinitrogen hydride species $[FeH(N_2)(P^2P_3{}^{Me})]^+$ ($P^2P_3{}^{Me} = P(CH_2CH_2PMe_2)_3$)[6b,32] and $[FeH(N_2)(P^2P_3{}^{iPr})]^+$ ($P^2P_3{}^{iPr} = P(CH_2CH_2PiPr_2)_3$),[7] and $[RuH(N_2)(P^2P_3{}^{Cy})]^+$ (**7**) is analogous to the known ruthenium(II) dinitrogen hydride species $[RuH(N_2)(P^2P_3{}^{iPr})]^+$.[7] These dinitrogen hydride complexes could also be formed through attack of a weak acid at the appropriate iron(0) and ruthenium(0) dinitrogen complex.

The $^{31}P\{^1H\}$ NMR spectra of complexes **6** and **7** exhibit the three characteristic resonances of an octahedral species with a tripodal tetradentate phosphine ligand. The central phosphine P_C signal of $[FeH(N_2)(P^2P_3{}^{Cy})]^+$ (**6**) at the relatively low field shift of 160.7 ppm is observed as a doublet of triplets with coupling constants of 28 and 24 Hz to P_T and P_E, respectively. The two equivalent terminal phosphines P_E exhibit a resonance at 79.8 ppm which appears as a doublet of doublets and has twice the intensity of the other signals for P_C and P_T. The coupling constant of P_E to P_T is 11 Hz. The resonance of P_T appears as a well resolved doublet of triplets at 70.3 ppm. The metal-bound hydride of **6** appears as a triplet of doublets of doublets at −14.62 ppm in the ^1H NMR spectrum, coupling to P_E, P_T, P_C with coupling constants of 69 Hz, 53 and 25 Hz respectively.

The $^{31}P\{^1H\}$ NMR spectra of $[RuH(N_2)(P^2P_3{}^{Cy})]^+$ (**7**) displays the central P_C signal at the low field shift of 140.7 ppm as a doublet of triplets with a coupling constants of 11 and 11 Hz to P_T and P_E, respectively. The two equivalent terminal phosphines P_E exhibit a resonance at 63.8 ppm which is observed as a doublet of doublets and has twice the intensity of the signals for P_C and P_T. The coupling constant of P_E to P_T is 11 Hz. The resonance of P_T appears as a well resolved doublet of triplets at 51.4 ppm. The metal-bound hydride of **7** appears as a double of triplets of doublets at −11.26 ppm in the ^1H NMR spectrum, coupling to P_T, P_E, and P_C with coupling constants of 72, 26, and 23 Hz respectively.

The infrared spectrum of $[FeH(N_2)(P^2P_3{}^{Cy})]^+$ (**6**) displays a sharp absorbance at 2107 cm^{-1}, and the spectrum of $[RuH(N_2)(P^2P_3{}^{Cy})]^+$ (**7**) displays a similar absorbance at 2172 cm^{-1}, both of which are assigned to the dinitrogen stretch $\nu(N{\equiv}N)$ for the respective complexes. These high values indicate the lower level of dinitrogen activation when bound to an Fe(II) or Ru(II) center when compared to the Fe(0), Ru(0), and Fe(I) dinitrogen complexes $Fe(N_2)(P^2P_3{}^{Cy})$ (**1**), $Fe(N_2)(P^2P_3{}^{Cy})$ (**2**), and $[Fe(N_2)(P^2P_3{}^{Cy})]^+$ (**3**) examined in this work. For this related series of iron complexes, the level of dinitrogen activation appears to decrease with increasing oxidation state, with the Fe(0) complex $Fe(N_2)(P^2P_3{}^{Cy})$ (**1**) having the greatest activation with an IR absorbance at 1996 cm^{-1}, followed by the Fe(I) complex $[Fe(N_2)(P^2P_3{}^{Cy})]^+$ (**3**) at 2059 cm^{-1} and finally the Fe(II) complex $[FeH(N_2)(P^2P_3{}^{Cy})]^+$ (**6**) at 2107 cm^{-1}. Similarly among the Ru complexes, the Ru(0) complex $Ru(N_2)(P^2P_3{}^{Cy})$ (**2**) has a $\nu(N{\equiv}N)$ of 2083 cm^{-1}, which is significantly more activated than its Ru(II) analogue $[RuH(N_2)(P^2P_3{}^{Cy})]^+$ (**7**) with a $\nu(N{\equiv}N)$ of 2172 cm^{-1}.

Crystals of $[FeH(N_2)(P^2P_3{}^{Cy})]^+$ (**6**) and $[RuH(N_2)(P^2P_3{}^{Cy})]^+$ (**7**) suitable for structural analysis were grown by vapor diffusion of pentane into THF solutions of **6**[**BF**$_4$] (Figure 10) and **7**[**BF**$_4$] (Figure 11). Selected bond angles and lengths are given in Tables 6 and 7 respectively.

The geometry for both $[FeH(N_2)(P^2P_3{}^{Cy})]^+$ (**6**) and $[RuH(N_2)(P^2P_3{}^{Cy})]^+$ (**7**) is distorted octahedral with the dinitrogen ligand located *trans* to the central phosphine of the phosphine ligand and the hydrido ligand located *trans* to one of the arm phosphines. The short N−N bond lengths of 1.028(7) Å for **6** and 1.069(4) Å for **7** indicate little, if any, activation of the nitrogen triple bond, consistent with the IR data.

Reaction of $[FeH(N_2)(P^2P_3{}^{Cy})]^+$ (**6**) with potassium *tert*-butoxide in THF results in the regeneration of $FeN_2(P^2P_3{}^{Cy})$ (**1**). A similar result was observed for *tert*-butoxide treatment of $[RuH(N_2)(P^2P_3{}^{Cy})]^+$ (**7**) in THF, with $Ru(N_2)(P^2P_3{}^{Cy})$ (**2**) being regenerated. The protonation of $FeN_2(P^2P_3{}^{Cy})$ (**1**) to give $[FeH(N_2)(P^2P_3{}^{Cy})]^+$ (**6**) is readily reversible (Scheme 6).

CONCLUSIONS

Successful synthetic routes to the iron(0) and ruthenium(0) dinitrogen complexes containing the bulky tetradentate $P^2P_3{}^{Cy}$ ligand were established. The increased steric bulk of the ligand set did not significantly alter the reactivity of these complexes when compared to that of their sterically less bulky analogues $M(N_2)(P^2P_3{}^{iPr})$ (M = Fe, Ru) and $Fe(N_2)(P^2P_3{}^{Me})$. Treatment with acid resulted in reversible protonation at the metal center to generate the hydrido nitrogen species $[FeH(N_2)(P^2P_3{}^{Cy})]^+$

dx.doi.org/10.1021/ic3024953 | Inorg. Chem. 2013, 52, 3043−3053

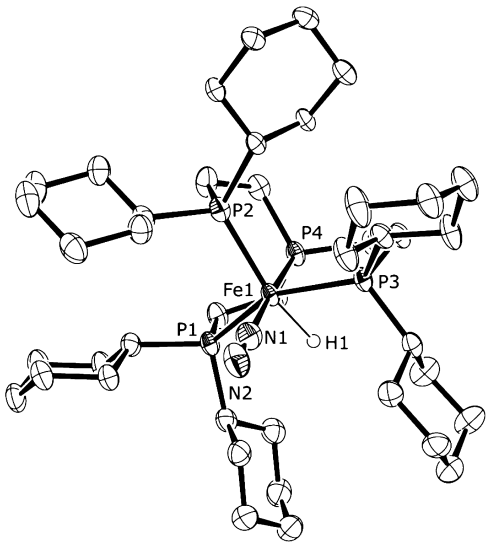

Figure 10. ORTEP plot (50% thermal ellipsoids) of $[FeH(N_2)(P^2P_3^{Cy})][BF_4]$ (**6**[BF_4]) within each asymmetric unit. Hydrogen atoms, tetrafluoroborate counterion, and THF solvate have been omitted for clarity.

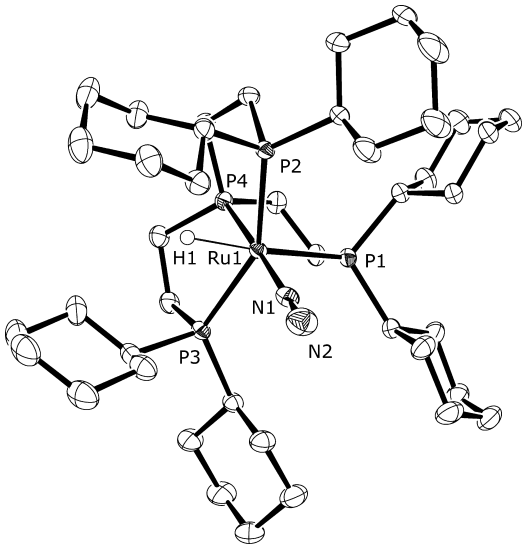

Figure 11. ORTEP plot (50% thermal ellipsoids) of $[RuH(N_2)(P^2P_3^{Cy})][BF_4]$ (**7**[BF_4]) within each asymmetric unit. Hydrogen atoms, tetrafluoroborate counterion, and THF solvate have been omitted for clarity.

Table 6. Selected Bond Lengths (Å) and Angles (°) for $[FeH(N_2)(P^2P_3^{Cy})][BF_4]$ (6[BF_4])

N1–N2	1.028(7)	Fe1–N1	1.859(6)
Fe1–P1	2.2723(15)	Fe1–P2	2.3033(17)
Fe1–P3	2.2481(15)	Fe1–P4	2.1752(16)
Fe1–H1	1.69(10)		
Fe1–N1–N2	179.7(7)	N1–Fe1–P1	94.27(15)
N1–Fe1–P2	98.06(17)	N1–Fe1–P3	93.50(15)
N1–Fe1–P4	176.87(17)	N1–Fe1–H1	103(3)
P1–Fe1–P2	102.88(6)	P1–Fe1–P3	148.12(6)
P1–Fe1–P4	84.56(5)	P1–Fe1–H1	77(4)
P2–Fe1–P3	106.55(6)	P2–Fe1–P4	85.04(6)
P2–Fe1–H1	159(3)	P3–Fe1–P4	86.02(6)
P3–Fe1–H1	71(4)	P4–Fe1–H1	74(3)

Table 7. Selected Bond Lengths (Å) and Angles (°) for $[RuH(N_2)(P^2P_3^{Cy})][BF_4]$ (7[BF_4])

N1–N2	1.069(4)	Ru1–N1	2.042(3)
Ru1–P1	2.4213(7)	Ru1–P2	2.3496(7)
Ru1–P3	2.3599(7)	Ru1–P4	2.2408(8)
Ru1–H1	1.65(4)		
Ru1–N1–N2	177.1(3)	N1–Ru1–P1	99.84(7)
N1–Ru1–P2	94.56(7)	N1–Ru1–P3	96.40(7)
N1–Ru1–P4	177.21(7)	N1–Ru1–H1	93.8(15)
P1–Ru1–P2	103.98(3)	P1–Ru1–P3	100.29(3)
P1–Ru1–P4	82.92(3)	P1–Ru1–H1	166.2(15)
P2–Ru1–P3	151.17(3)	P2–Ru1–P4	84.42(3)
P2–Ru1–H1	76.1(15)	P3–Ru1–P4	83.36(3)
P3–Ru1–H1	76.7(15)	P4–Ru1–H1	83.4(15)

Scheme 6

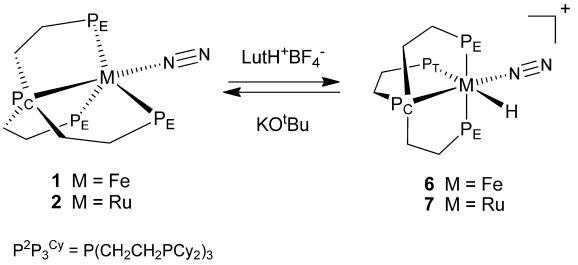

(**6**) and $[RuH(N_2)(P^2P_3^{Cy})]^+$ (**7**). No reaction at the coordinated dinitrogen ligand was observed.

The extra steric bulk of the $P^2P_3^{Cy}$ ligand did permit the generation and characterization of stable iron(I) and ruthenium(I) species $[Fe(N_2)(P^2P_3^{Cy})]^+$ (**3**) and $RuCl(P^2P_3^{Cy})$ (**4**), and these are among the very few Fe(I) and Ru(I) species to be isolated and characterized. The increased steric bulk of the $P^2P_3^{Cy}$ ligand conveys additional stability to the complexes, probably by restricting the disproportionation pathways which contribute to the instability of most iron(I) and ruthenium(I) species.

In terms of activation of coordinated dinitrogen, it is clear from the compounds synthesized in this work that the level of dinitrogen activation, i.e., weakening of the N–N bond reflected by the $\nu(N{\equiv}N)$ in the infrared spectra, is greater with the lower oxidation states of the metal centers. The Fe(0) and Ru(0) complexes had significantly weaker N≡N bonds than their Fe(II) and Ru(II) analogues with the Fe(I) dinitrogen complex midway between the Fe(0) and Fe(II) complexes.

EXPERIMENTAL SECTION

General Information. All manipulations were carried out using standard Schlenk, vacuum and glovebox techniques under a dry atmosphere of nitrogen. Solvents were dried, distilled under nitrogen or argon using standard procedures,[33] and stored in glass ampules fitted with J. Young Teflon taps. Benzene was dried over sodium wire before distillation from sodium/benzophenone. THF (inhibitor free), toluene, and pentane were dried and deoxygenated using a Pure Solv 400-4-MD (Innovative Technology) solvent purification system. Deuterated solvents THF-d_8, toluene-d_8 and benzene-d_6 were dried over, and distilled from sodium/benzophenone and were vacuum distilled immediately prior to use. Potassium graphite,[34] potassium triethylborohydride,[35] lutidinium tetrafluoroborate,[36] $P^2P_3^{Cy}$,[9] $[RuCl(P^2P_3^{Cy})][BPh_4]$,[9] $[RuCl(P^2P_3^{Cy})][Cl]$,[9] and $[FeCl(P^2P_3^{Cy})][BPh_4]$[9] were prepared by literature methods. Potassium *tert*-butoxide was purchased from Sigma-Aldrich, sublimed twice, and then stored under

dx.doi.org/10.1021/ic3024953 | Inorg. Chem. 2013, 52, 3043–3053

Table 8. Crystal Data Refinement Details for [RuCl(P²P₃Cy)][BPh₄], 1, 2, 3[BPh₄], 4, 5, 6[BF₄], and 7[BF₄]

	[RuCl(P²P₃Cy)][BPh₄]	1	2	3[BPh₄]	4	5	6[BF₄]	7[BF₄]
chemical formula	$C_{70}H_{106}BClOP_4Ru$	$C_{44.50}H_{84}N_2P_4Ru$	$C_{45}H_{81}FeN_2P_4$	$C_{66}H_{96}BFeN_2P_4$	$C_{44.50}H_{83}ClP_4Ru$	$C_{42}H_{80}FeP_4$	$C_{88}H_{166}B_2F_8Fe_2N_4OP_8$	$C_{44}H_{82}BF_4N_2OP_4Ru$
formula mass	1234.76	872.09	829.85	1107.99	878.51	764.79	1829.33	966.88
crystal system	monoclinic	monoclinic	triclinic	triclinic	monoclinic	triclinic	triclinic	triclinic
a/Å	13.3779(5)	13.6360(5)	13.669(3)	12.7369(11)	13.905(2)	13.7011(9)	10.164(2)	10.3846(3)
b/Å	14.0391(6)	14.2697(5)	13.689(3)	14.0990(13)	26.160(5)	16.1969(11)	13.584(3)	13.8215(4)
c/Å	34.5248(14)	23.6883(7)	14.026(3)	17.5151(17)	14.691(3)	19.7521(13)	18.239(4)	18.2337(6)
α/°	90.00	90.00	96.14(3)	79.842(5)	90.00	80.320(3)	85.44(3)	84.1190(10)
β/°	96.731(2)	90.5590(10)	96.77(3)	75.048(5)	114.028(8)	83.021(3)	78.68(3)	75.7350(10)
γ/°	90.00	90.00	119.69(3)	83.820(5)	90.00	78.371(3)	83.89(3)	86.2970(10)
V/Å³	6439.5(4)	4609.1(3)	2222.0(8)	2984.8(5)	4880.9(15)	4214.7(5)	2450.8(8)	2520.95(13)
temperature/K	155(2)	152(2)	100(2)	154(2)	160(2)	155(2)	100(2)	155(2)
space group	$P2(1)/c$	P2(1)/n	$P\bar{1}$	$P\bar{1}$	$P21/c$	$P\bar{1}$	$P\bar{1}$	$P\bar{1}$
Z	4	4	2	2	4	4	1	2
μ(Mo Kα) (mm^{-1})	46797	40047	28651	39524	35186	55487	31485	41115
N	11278	10047	7306	10247	8604	14758	8092	8846
N_{ind}	0.0912	0.0409	0.0250	0.0880	0.1575	0.0572	0.0515	0.0366
R_{int}	0.0485	0.0268	0.0436	0.0696	0.0715	0.0409	0.0717	0.0360
final R_1 values ($I > 2\sigma(I)$)	0.1183	0.0614	0.1087	0.1760	0.1636	0.0825	0.1985	0.1015
final $wR(F^2)$ values ($I > 2\sigma(I)$)	0.0973	0.0390	0.0460	0.1491	0.1778	0.0789	0.0849	0.0403
final R_1 values (all data)	0.1511	0.0670	0.1105	0.2126	0.2152	0.0970	0.2077	0.1058

dx.doi.org/10.1021/ic3024953 | Inorg. Chem. 2013, 52, 3043−3053

an inert atmosphere prior to use. Air-sensitive NMR samples were prepared in an argon- or nitrogen-filled glovebox or on a high vacuum line by vacuum transfer of solvent into an NMR tube fitted with a concentric Teflon valve. ^{1}H and $^{31}P\{^{1}H\}$ NMR spectra were recorded on Bruker Avance III 300, Avance III 400 or Avance III 600 NMR spectrometers operating at 300.3, 400.13, and 600.13 MHz for ^{1}H, and 121.49, 161.98, and 242.95 MHz for $^{31}P\{^{1}H\}$ respectively. All NMR spectra were recorded at 298 K, unless otherwise stated. ^{1}H NMR spectra were referenced to residual solvent resonances. $^{31}P\{^{1}H\}$ NMR spectra were referenced to external neat trimethylphosphite at 140.85 ppm, and $^{15}N\{^{1}H\}$ NMR spectra were reference to external neat nitromethane at 0 ppm.

Microanalyses were carried out at the Campbell Microanalytical Laboratory, University of Otago, New Zealand. Details of the X-ray analyses are given in Table 8.

Synthesis of $Fe(N_2)(P^2P_3^{Cy})$ (1). Potassium graphite (76 mg, 0.56 mmol) was added to a solution of $[FeCl(P^2P_3^{Cy})][BPh_4]$ (270 mg, 0.242 mmol) in THF (approximately 15 mL). The reaction mixture was stirred under nitrogen for 20 h. The resulting black suspension was filtered to give an orange solution. The solvent was removed under reduced pressure, and the solid residue was extracted into benzene (approximately 10 mL). The orange solution was filtered and then reduced to around 1 mL under reduced pressure to precipitate $Fe(N_2)(P^2P_3^{Cy})$ (**1**) as a red/orange solid (63 mg, 0.080 mmol, 33%). Anal. Found. C 64.17, H 9.65, N 2.47, $C_{42}H_{78}FeN_2P_4$ (MW 790.837) requires C 63.79, H 9.94, N 3.54. Elemental analysis performed on the crystalline product suggests some loss of weakly bound dinitrogen ligand upon application of vacuum during analytical procedure, consistent for complexes of this type.[7] $^{31}P\{^{1}H\}$ NMR (121 MHz, benzene-d_6): δ 175.3 (1P, q, $^{2}J_{P-P}$ = 36 Hz, $\mathbf{P_C}$); 84.2 (3P, d, $^{2}J_{P-P}$ = 36 Hz, $\mathbf{P_E}$). ^{1}H NMR (400 MHz, benzene-d_6): δ 2.29 (4H, m, C$\mathbf{H_2}^{arm}$); 2.13 (8H, m, $\mathbf{CH_2}^{arm}$); 2.0−1.7 (26H, m, Cy**H**); 1.48 (24H, m, Cy**H**); 1.4−1.1 (16H, m, Cy**H**). IR (fluorolube): 1996 s, ν(N≡N) cm^{-1}.

Synthesis of $Ru(N_2)(P^2P_3^{Cy})$ (2). Potassium graphite (80 mg, 0.59 mmol) was added to a suspension of $[RuCl(P^2P_3^{Cy})]Cl$ (125 mg, 0.142 mmol) in THF (approximately 15 mL). The reaction mixture was stirred under nitrogen for 18 h, after which it was filtered to afford a dark yellow solution. The solvent was removed under reduced pressure, and the resulting dark yellow solid was dissolved in pentane and filtered and the solvent removed under reduced pressure once more to afford $Ru(N_2)(P^2P_3^{Cy})$ (**2**) (41 mg, 0.049 mmol, 35%) as an orange solid. Anal. Found. C 60.13, H 9.57, N 2.92, $C_{42}H_{78}N_2P_4Ru$ (MW 843.50) requires C 60.34, H 9.40, N 3.35. $^{31}P\{^{1}H\}$ NMR (121 MHz, benzene-d_6): δ 160.7 (1P, q, $^{2}J_{P-P}$ = 22 Hz, $\mathbf{P_C}$); 73.9 (3P, d, $^{2}J_{P-P}$ = 22 Hz, $\mathbf{P_E}$). ^{1}H NMR (300 MHz, benzene-d_6): δ 2.1−1.6 (42H, m, C$\mathbf{H_2}^{arm}$/Cy**H**); 1.6−1.1 (36H, m, Cy**H**). IR (fluorolube): 2083 s, ν(N≡N) cm^{-1}.

Synthesis of $Ru(^{15}N_2)(P^2P_3^{Cy})$ ($^{15}N_2$-2). $Ru(N_2)(P^2P_3^{Cy})$ (**2**) (approximately 40 mg, 50 μmol) was dissolved in benzene-d_6 (0.5 mL) in an NMR tube fitted with a concentric Teflon valve under dinitrogen. The solution was degassed with three freeze−pump−thaw cycles before the introduction of $^{15}N_2$ into the NMR tube headspace. NMR spectra indicated the successful exchange of the dinitrogen ligand following thawing of the solution and warming to room temperature. $^{31}P\{^{1}H\}$ NMR (162 MHz, benzene-d_6): δ 160.8 (1P, dqd, $^{2}J_{P-N}$ = 31 Hz, $^{2}J_{P-P}$ = 22 Hz, $^{3}J_{P-N}$ = 3 Hz, $\mathbf{P_C}$); 74.0 (3P, ddd, $^{2}J_{P-P}$ = 22 Hz, $^{2}J_{P-N}$ = 5 Hz, $^{3}J_{P-N}$ = 2 Hz, $\mathbf{P_E}$). $^{15}N\{^{1}H\}$ NMR (40.56 MHz, benzene-d_6): δ −9.0 (1N, s br, $\mathbf{N_\beta}$); −52.5 (1N, dqd, $^{2}J_{N-P}$ = 31 Hz, $^{2}J_{N-P}$ = 5 Hz, $^{1}J_{N-N}$ = 5 Hz, $\mathbf{N_\alpha}$).

Synthesis of $[Fe(N_2)(P^2P_3^{Cy})][BPh_4]$ (3[BPh4]). Potassium graphite (17 mg, 0.13 mmol) was added to a solution of $[FeCl(P^2P_3^{Cy})][BPh_4]$ (132 mg, 0.118 mmol) in THF (approximately 15 mL). The reaction mixture was stirred under nitrogen for 20 h. The resulting black suspension was filtered to give a dark red solution. The solvent was removed under reduced pressure, and the solid residue washed with pentane (approximately 20 mL). The red solid was collected by filtration to afford $[Fe(N_2)(P^2P_3^{Cy})][BPh_4]$ (**3[BPh4]**) (58 mg, 0.052 mmol, 44%). Anal. Found. C 71.15, H 9.05, N 2.07, $C_{66}H_{98}BFeN_2P_4$ (MW 1110.05) requires C 71.41, H 8.90, N 2.52. IR (fluorolube): 2059 s, ν(N≡N) cm^{-1}.

Synthesis of $RuCl(P^2P_3^{Cy})$ (4). Potassium graphite (18 mg, 0.13 mmol) was added to a solution of $[RuCl(P^2P_3^{Cy})][Cl]$ (102 mg, 0.116 mmol) in THF (approximately 15 mL). The reaction mixture was stirred under nitrogen for 20 h. The resulting black suspension was filtered to give a very dark solution. The solvent was removed under reduced pressure, and the solid residue extracted with pentane (approximately 30 mL). The solution was then filtered to give a deep blue filtrate. The volume of the solution was reduced to 5 mL and allowed to stand overnight, resulting in the precipitation of a blue solid which was collected by filtration to afford $RuCl(P^2P_3^{Cy})$ (**4**) (72 mg, 0.085 mmol, 74%). Anal. Found. C 59.91, H 9.51, $C_{42}H_{78}ClP_4Ru$ (MW 843.50) requires C 59.81, H 9.32.

Synthesis of $Fe(H)_2(P^2P_3^{Cy})$ (5). Potassium triethylborohydride (35 mg, 0.25 mmol) was added to a stirring suspension of $[FeCl(P^2P_3^{Cy})][BPh_4]$ (120 mg, 0.107 mmol) in toluene (10 mL) which was stirred under nitrogen for 3 h. Volatiles were removed under reduced pressure. The orange residue was extracted with pentane (30 mL) and the resultant solution was filtered and volatiles removed to afford $Fe(H)_2(P^2P_3^{Cy})$ (**5**) (57 mg, 0.075 mmol, 70% yield) as an orange solid. Anal. Found. C 66.21, H 10.39, $C_{42}H_{80}FeP_4$ (MW 764.84) requires C 65.96, H 10.54. $^{31}P\{^{1}H\}$ NMR (162 MHz, benzene-d_6): δ 174.4 (1P, q, $^{2}J_{P-P}$ = 18 Hz, $\mathbf{P_C}$); 102.3 (3P, d, $^{2}J_{P-P}$ = 18 Hz, $\mathbf{P_E}/\mathbf{P_T}$). ^{1}H NMR (300 MHz, benzene-d_6): δ 2.39 (4H, m, C$\mathbf{H_2}^{arm}$); 2.1−1.6 (32H, m, C$\mathbf{H_2}^{arm}$/Cy**H**); 1.6−1.1 (42H, m, Cy**H**); −12.84 (2H, qd, $^{2}J_{H-P}$ = 46 Hz, $^{2}J_{H-P}$ = 3 Hz, Fe**H**). $^{31}P\{^{1}H\}$ NMR (243 MHz, toluene-d_8, 190 K): δ 175.0 (1P, s br, $\mathbf{P_C}$); 113.7 (1P, s br, $\mathbf{P_T}$); 96.8 (2P, s br, $\mathbf{P_E}$). ^{1}H NMR (600 MHz, toluene-d_8, 190 K, high field only): δ −7.98 (1H, s br, Fe**H**); −17.67 (1H, s br, Fe**H**).

Synthesis of $[FeH(N_2)(P^2P_3^{Cy})][BF_4]$ (6[BF$_4$]). A solution of lutidinium tetrafluoroborate (23 mg, 0.12 mmol) in THF (5 mL) was added to a solution of $Fe(H)_2(P^2P_3^{Cy})$ (**5**) (85.0 mg, 0.111 mmol) in THF (20 mL), and the reaction mixture was stirred overnight under nitrogen, resulting in a color change from pale orange to a darker pink/orange. The solution was filtered through Celite and reduced in volume to 4 mL under reduced pressure. The addition of pentane (30 mL) resulted in the precipitation of a tan solid which was collected by filtration to afford $[FeH(N_2)(P^2P_3^{Cy})][BF_4]$ (**6[BF$_4$]**) (58 mg, 0.066 mmol, 59%). Anal. found C 57.35, H 9.19, N 2.57, $C_{42}H_{79}BF_4FeN_2P_4$ (MW 878.649) requires C 57.41, H9.06, N 3.19. Elemental analysis performed on the crystalline product suggests some loss of weakly bound dinitrogen ligand upon application of vacuum during analytical procedure. $^{31}P\{^{1}H\}$ NMR (162 MHz, THF-d_8): δ 160.7 (1P, dt, $^{2}J_{PC-PT}$ = 28 Hz, $^{2}J_{PC-PE}$ = 24 Hz, $\mathbf{P_C}$); 79.8 (2P, dd, $^{2}J_{PE-PC}$ = 24 Hz, $^{2}J_{PE-PT}$ = 11 Hz, $\mathbf{P_E}$); 70.3 (1P, dt, $^{2}J_{PT-PC}$ = 28 Hz, $^{2}J_{PT-PE}$ = 11 Hz, $\mathbf{P_T}$). ^{1}H NMR (400 MHz, THF-d_8): δ 2.7−2.2 (12H, m, C$\mathbf{H_2}^{arm}$); 2.2−1.1 (66H, m, Cy**H**); −14.62 (1H, tdd, $^{2}J_{H-P}$ = 69 Hz, $^{2}J_{H-P}$ = 53 Hz, $^{2}J_{H-P}$ = 25 Hz, Fe**H**). IR (fluorolube): 2107 s, ν(N≡N) cm^{-1}.

Synthesis of $[RuH(N_2)(P^2P_3^{Cy})][BF_4]$ (7[BF$_4$]). Solid lutidinium tetrafluoroborate (11 mg, 0.056 mmol) was added to a stirred solution of $Ru(N_2)(P^2P_3^{Cy})$ (**2**) (45 mg, 0.054 mmol) in THF (20 mL). The solution was pale green in color after 3 min but then turned to a pale orange after one hour. The volume of the solution was reduced to ∼5 mL under reduced pressure before pentane (30 mL) was added resulting in the precipitation of a pale orange solid. This solid was collected by filtration to afford $[RuH(N_2)(P^2P_3^{Cy})][BF_4]$ (**7[BF$_4$]**) (40 mg, 0.043 mmol, 80%). Anal. Found. C 54.39, H 8.46, N 2.02, $C_{42}H_{79}BF_4N_2P_4Ru$ (MW 923.87) requires C 54.60, H 8.62, N 3.03. Elemental analysis performed on the crystalline product suggests some loss of weakly bound dinitrogen ligand upon application of vacuum during analytical procedure. $^{31}P\{^{1}H\}$ NMR (243 MHz, THF-d_8): δ 140.7 (1P, dt, $^{2}J_{P-P}$ = 11 Hz, $^{2}J_{P-P}$ = 11 Hz, $\mathbf{P_C}$); 63.8 (2P, dd, $^{2}J_{P-P}$ = 11 Hz, $^{2}J_{P-P}$ = 11 Hz, $\mathbf{P_E}$); 51.4 (1P, dt, $^{2}J_{P-P}$ = 11 Hz, $^{2}J_{P-P}$ = 11 Hz, $\mathbf{P_T}$). ^{1}H NMR (600 MHz, THF-d_8): δ 2.55 (4H, m); 2.22 (2H, m); 2.12 (4H, m); 2.01 (4H, m); 1.92−1.65 (30H, m); 1.65−1.47 (14H, m); 1.47−1.20 (20H, m); −11.26 (1H, dtd, $^{2}J_{H-P}$ = 72 Hz, $^{2}J_{H-P}$ = 26 Hz, $^{2}J_{H-P}$ = 23 Hz, Ru**H**). IR (fluorolube): 2172 s, ν(N≡N) cm^{-1}.

dx.doi.org/10.1021/ic3024953 | Inorg. Chem. 2013, 52, 3043−3053

■ ASSOCIATED CONTENT

Supporting Information

CIF files for complexes **1**, **2**, **3**[BPh_4], **4**, **5**, **6**[BPh_4], and **7**[BPh_4]. Data for the solid state structure of [RuCl($P^2P_3^{Cy}$)][BPh_4] as well as information on EPR simulations is also included. This material is available free of charge via the Internet at http://pubs.acs.org.

■ AUTHOR INFORMATION

Corresponding Author

*E-mail: L.Field@unsw.edu.au. Telephone: +61 2 9385 2700.

Author Contributions

The manuscript was written through contributions of all authors. All authors have given approval to the final version of the manuscript.

Notes

The authors declare no competing financial interest.

■ ACKNOWLEDGMENTS

The authors wish to thank Dr. Hsiu Lin Li and Dr. Alison Magill from the School of Chemistry at the University of New South Wales for technical assistance, proof reading, and discussions. The authors also thank the Australian Research Council for financial support, and R.G.W. thanks the Australian Government and the University of New South Wales for postgraduate scholarships. NMR spectra were obtained through the Mark Wainwright Analytical Center at the University of New South Wales, and subsidized access to these facilities is gratefully acknowledged.

■ REFERENCES

(1) Allen, A. D.; Senoff, C. W. *Chem. Commun.* **1965**, 621−2.

(2) (a) Fryzuk, M. D.; Johnson, S. A. *Coord. Chem. Rev.* **2000**, *200*−*202*, 379−409. (b) Hidai, M. *Coord. Chem. Rev.* **1999**, *185*−*186*, 99−108. (c) MacKay, B. A.; Fryzuk, M. D. *Chem. Rev.* **2004**, *104*, 385−401.

(3) (a) Laplaza, C. E.; Cummins, C. C. *Science* **1995**, *268*, 861−3. (b) George, T. A.; Rose, D. J.; Chang, Y.; Chen, Q.; Zubieta, J. *Inorg. Chem.* **1995**, *34*, 1295−8. (c) Yandulov, D. V.; Schrock, R. R. *J. Am. Chem. Soc.* **2002**, *124*, 6252−6253. (d) Betley, T. A.; Peters, J. C. *J. Am. Chem. Soc.* **2004**, *126*, 6252−6254. (e) Fryzuk, M. D.; Johnson, S. A.; Patrick, B. O.; Albinati, A.; Mason, S. A.; Koetzle, T. F. *J. Am. Chem. Soc.* **2001**, *123*, 3960−3973.

(4) We have adopted a shorthand convention for PP_3 ligands $P^nP_3^X$ where *n* designates the number of carbons in the chains linking the central and terminal phophines and *X* identifies the substituents on the terminal phosphines. Hence $P^3P_3^{Me}$ would refer to the complex $P(CH_2CH_2CH_2PMe_2)_3$ with 3-carbon straps between the central and terminal phosphines and methyl substituents on the terminal phosphines.

(5) (a) Bianchini, C.; Laschi, F.; Peruzzini, M.; Zanello, P. *Gazz. Chim. Ital.* **1994**, *124*, 271−5. (b) King, R. B.; Kapoor, R. N.; Saran, M. S.; Kapoor, P. N. *Inorg. Chem.* **1971**, *10*, 1851−60. (c) Stoppioni, P.; Mani, F.; Sacconi, L. *Inorg. Chim. Acta* **1974**, *11*, 227−30.

(6) (a) Field, L. D.; Messerle, B. A.; Smernik, R. J.; Hambley, T. W.; Turner, P. *Inorg. Chem.* **1997**, *36*, 2884−2892. (b) Field, L. D.; Messerle, B. A.; Smernik, R. J. *Inorg. Chem.* **1997**, *36*, 5984−5990.

(7) Field, L. D.; Guest, R. W.; Vuong, K. Q.; Dalgarno, S. J.; Jensen, P. *Inorg. Chem.* **2009**, *48*, 2246−2253.

(8) Gilbert-Wilson, R.; Field, L. D.; Bhadbhade, M. M. *Inorg. Chem.* **2012**, *51*, 3239−46.

(9) Jia, G.; Drouin, S. D.; Jessop, P. G.; Lough, A. J.; Morris, R. H. *Organometallics* **1993**, *12*, 906−16.

(10) Leigh, G. J.; Jimenez-Tenorio, M. *J. Am. Chem. Soc.* **1991**, *113*, 5862−3.

(11) Gilbertson, J. D.; Szymczak, N. K.; Tyler, D. R. *J. Am. Chem. Soc.* **2005**, *127*, 10184−10185.

(12) Field, L. D.; Messerle, B. A.; Smernik, R. J. *Inorg. Chem.* **1997**, *36*, 5984−5990.

(13) Donovan-Mtunzi, S.; Richards, R. L.; Mason, J. *J. Chem. Soc., Dalton Trans.* **1984**, 469−474.

(14) Otting, G.; Messerle, B. A.; Soler, L. P. *J. Am. Chem. Soc.* **1997**, *119*, 5425−5434.

(15) Addison, A. W.; Rao, T. N.; Reedijk, J.; Vanrijn, J.; Verschoor, G. C. *J. Chem. Soc., Dalton Trans.* **1984**, 1349−1356.

(16) Sutton, L. E. *Tables of Interatomic Distances and Configuration in Molecules and Ions*; The Chemical Society: London, 1958.

(17) Komiya, S.; Akita, M.; Yoza, A.; Kasuga, N.; Fukuoka, A.; Kai, Y. *J. Chem. Soc., Chem. Commun.* **1993**, 787−788.

(18) Hazari, N. *Chem. Soc. Rev.* **2010**, *39*, 4044−4056.

(19) Hughes, D. L.; Leigh, G. J.; Jimenez-Tenorio, M.; Rowley, A. T. *J. Chem. Soc., Dalton Trans.* **1993**, 75−82.

(20) Fryzuk, M. D.; Johnson, S. A. *Coord. Chem. Rev.* **2000**, *200*−*202*, 379−409.

(21) Zotti, G.; Pilloni, G.; Bressan, M.; Martelli, M. *J. Electroanal. Chem. Interf.* **1977**, *75*, 607−612.

(22) Takaoka, A.; Gerber, L. C. H.; Peters, J. C. *Angew. Chem., Int. Ed.* **2010**, *49*, 4088−4091.

(23) Mankad, N. P.; Whited, M. T.; Peters, J. C. *Angew. Chem., Int. Ed.* **2007**, *46*, 5768−5771.

(24) Scott, J.; Vidyaratne, I.; Korobkov, I.; Gambarotta, S.; Budzelaar, P. H. M. *Inorg. Chem.* **2008**, *47*, 896−911.

(25) (a) Lu, C. C.; Bill, E.; Weyhermüller, T.; Bothe, E.; Wieghardt, K. *J. Am. Chem. Soc.* **2008**, *130*, 3181−3197. (b) Harkins, S. B.; Mankad, N. P.; Miller, A. J. M.; Szilagyi, R. K.; Peters, J. C. *J. Am. Chem. Soc.* **2008**, *130*, 3478−3485. (c) Adhikari, D.; Mossin, S.; Basuli, F.; Huffman, J. C.; Szilagyi, R. K.; Meyer, K.; Mindiola, D. J. *J. Am. Chem. Soc.* **2008**, *130*, 3676−3682.

(26) (a) de Bruin, B.; Hetterscheid, D. G. H. *Eur. J. Inorg. Chem.* **2007**, *2007*, 211−230. (b) Ghumaan, S.; Sarkar, B.; Patra, S.; van Slageren, J.; Fiedler, J.; Kaim, W.; Lahiri, G. K. *Inorg. Chem.* **2005**, *44*, 3210−3214.

(27) Miyazato, Y.; Wada, T.; Muckerman, J. T.; Fujita, E.; Tanaka, K. *Angew. Chem.* **2007**, *119*, 5830−5832.

(28) Büttner, T.; Geier, J.; Frison, G.; Harmer, J.; Calle, C.; Schweiger, A.; Schönberg, H.; Grützmacher, H. *Science* **2005**, *307*, 235−238.

(29) Cataldo, L.; Choua, S.; Berclaz, T.; Geoffroy, M.; Mézailles, N.; Avarvari, N.; Mathey, F.; Le Floch, P. *J. Phys. Chem. A* **2002**, *106*, 3017−3022.

(30) Sarkar, B.; Kaim, W.; Fiedler, J.; Duboc, C. *J. Am. Chem. Soc.* **2004**, *126*, 14706−14707.

(31) (a) Lobkovskii, E. B.; A., M. Y.; Borisov, A. P.; Makhaev, V. D.; Semenenko, K. N.; Struchkov, Yu.T. *Koord. Khim.* **1980**, *6*, 1267. (b) Guggenberger, L. J.; Titus, D. D.; Flood, M. T.; Marsh, R. E.; Orio, A. A.; Gray, H. B. *J. Am. Chem. Soc.* **1972**, *94*, 1135−1143. (c) Gao, Y.; Holah, D. G.; Hughes, A. N.; Spivak, G. J.; Havighurst, M. D.; Magnuson, V. R.; Polyakov, V. *Polyhedron* **1997**, *16*, 2797−2807.

(32) Field, L. D.; Guest, R. W.; Turner, P. *Inorg. Chem.* **2010**, *49*, 9086−9093.

(33) Perrin, D. D., Armarego, W. L. F. *Purification of Laboratory Chemicals*, 3rd ed.; Pergamon Press: Oxford, 1993.

(34) Weitz, I. S.; Rabinovitz, M. *J. Chem. Soc., Perkin Trans. 1* **1993**, *1*, 117−120.

(35) Brown, C. A.; Krishnamurthy, S. *J. Organomet. Chem.* **1978**, *156*, 111−21.

(36) Ohmori, H.; Takanami, T.; Shimada, H.; Masui, M. *Chem. Pharm. Bull.* **1987**, *35*, 2558−60.